

## Late-time behavior of stellar collapse and explosions:

### I. Linearized perturbations

Carsten Gundlach, Richard H. Price and Jorge Pullin

*Department of Physics, University of Utah, Salt Lake City, UT 84112-1195*

(9 July, 1993)

#### Abstract

We study the power-law tails in the evolution of massless fields around a fixed background geometry corresponding to a black hole. We give analytical arguments for their existence at  $scri_+$ , at the future horizon and at future timelike infinity. We confirm their existence with numerical integrations of the curved spacetime wave equation on the background of a Schwarzschild and a Reissner-Nordström black hole. These results are relevant to studies of mass inflation and the instability of Cauchy horizons. The analytic arguments also suggest the behavior of the full nonlinear dynamics, which we study numerically in a companion paper.

## I. INTRODUCTION

In the study of nonspherical gravitational collapse, the late stages of black hole formation and nonspherical stellar dynamics, certain simplifications have been traditional. Typically, linearized perturbation theory has been used on a fixed background, and the results have been taken to be representative of nonperturbative collapse.

One of the most basic results [1–3] about the evolution of fields on a curved background is that “sandwich waves” are not usually possible. At late times waves do not cut off sharply but die off in “tails.”

In the context of perturbations of spherical objects, like stars or black holes, arguments have been given [4] leading to the conclusion that the tails have a specific power-law form. The intention of this paper is to analyze in detail in which regions of the spacetime this form for the tails holds and under what conditions they develop.

In section II we start by giving an analytical outline of the development of tails in spherically symmetric fixed backgrounds. We present a somewhat more general and more pedagogical derivation of the results of the appendix of reference [4]. Moreover, we give two new results:

1) We show that for perturbations around a black hole, power-law tails develop not only at timelike infinity as was proven in [4] but also at  $scri_+$  and at the black-hole horizon. This result is of relevance since the development of tails in these regions is crucial for the physics of mass inflation [5] and the stability of Cauchy horizons. At least twice [6,7] in the literature it has been stated that the power-law tails are “nonradiative,” suggesting that the tails made no appearance at  $scri_+$  or at the horizon.

2) Generalizing the arguments for the Schwarzschild background, we show that power-law tails develop even when no horizon is present in the background. This would mean, among other things, that power-law tails should be present in perturbations of stars, or after the implosion and subsequent explosion of a massless field which does not result in black hole formation.

In sections III and IV we confirm the first of these results for the Schwarzschild background by performing numerical integrations of the perturbation equations for different initial shapes and different multipole moments of the field. We also confirm that the results extend to the case of Reissner-Nordström black holes; this is the first clear evidence that power-law tails actually develop for the background of direct relevance to mass inflation and stability of Cauchy horizons. Section III contains a brief discussion of our numerical method; section IV contains our numerical results.

In section V we make some final remarks, especially about possible implications, both for the behavior of test fields evolving on a time-dependent stellar collapse or explosion background, and for the behavior of a (spherically symmetric) self-gravitating massless field in a collapse or explosion situation. We develop this subject in a subsequent paper.

Tails have also been found important in the detailed calculation of gravitational waveforms from the inspiral collapse of binary systems. The tail back reaction appears as a correction to the 3/2 Post Newtonian equations of motions [8].

## II. SCHWARZSCHILD BACKGROUND AND BEYOND

In this section we examine the evolution of massless perturbation fields outside a star collapsing to form a black hole. We make the idealization that the mass loss in the transition from star to black hole can be neglected. (If there are massless perturbation fields outside the star at all, they will carry some energy away to null infinity, but we neglect this compared to the mass of the star.) If the star is spherically symmetric (again neglecting the perturbation fields, which need not be spherically symmetric), spacetime outside the star is Schwarzschild spacetime. We are therefore dealing with the (massless) wave equation on a region of Schwarzschild spacetime given by

$$ds^2 = - \left(1 - \frac{2M}{r}\right) dt^2 + \left(1 - \frac{2M}{r}\right)^{-1} dr^2 + r^2(d\theta^2 + \sin^2\theta d\phi^2), \quad (1)$$

where we have used  $c = G = 1$  units. We introduce a “tortoise” radial coordinate  $r_* \equiv r + 2M \ln(r - 2M)$ , advanced time  $v \equiv t + r_*$ , and retarded time  $u \equiv t - r_*$ , in terms of

which the line element becomes

$$ds^2 = -\left(1 - \frac{2M}{r}\right)dudv + r^2(d\theta^2 + \sin^2\theta d\phi^2). \quad (2)$$

We let the star begin its collapse at retarded time  $u = u_0$ . The characteristic  $u = u_0$  will be one boundary for our problem.

After the surface has started collapsing, it rapidly approaches the speed of light. The worldline of the stellar surface is therefore asymptotic to an ingoing null geodesic  $v = v_0$ . It is convenient to consider this  $v = v_0$  null geodesic, rather than the stellar surface, as the left boundary of the problem, and the data on this line for  $u > u_0$  to complete the specification of the problem. The variation of  $\phi$  on the stellar surface is asymptotically infinitely redshifted. (See [4] for details.) This means that  $\phi_{,u}$  will be small (more precisely, exponentially small) at late times and we make the specific assumption that, after some retarded time  $u = u_1$ , variations in  $\phi$  on  $v = v_0$  can be ignored. This black hole formation scenario is illustrated in Fig. 1.

Since the background is spherically symmetric, each multipole of a perturbation field evolves separately. For a scalar field  $\phi(t, r, \theta, \varphi)$ , for example, we can write  $\phi = \sum_{l,m} \Psi_m^l(u, r) Y_l^m(\theta, \varphi)/r$  and for each multipole moment we have

$$-4\Psi_{,uv} = V_l(r)\Psi, \quad V_l \equiv \left(1 - \frac{2M}{r}\right) \left(\frac{l(l+1)}{r^2} + R(r)\right), \quad (3)$$

where  $R(r)$  falls off as  $r^{-3}$  for large  $r$ , and where we have suppressed the indices  $l, m$  on  $\Psi$ . The evolutions of scalar, electromagnetic, and gravitational perturbations are all governed by an equation with the form of (3). Only the details of  $R(r)$  differ from one type of field to another.

The general solution to (3) can be written as a series depending on two arbitrary functions  $F$  and  $G$ :

$$\Psi = \sum_{p=0}^l A_l^p r^{-p} \left[ (G^{(l-p)}(u) + (-1)^p F^{(l-p)}(v)) \right] + \sum_{p=0}^{\infty} B_l^p(r) \left[ (G^{(l-p-1)}(u) + (-1)^p F^{(l-p-1)}(v)) \right], \quad (4)$$

where the superindices on  $F$  and  $G$  indicate the number of times the function is differentiated; negative superindices are to be interpreted as integrals. The coefficients  $A_l^p$  are dimensionless fixed numbers which have the same values as in flat spacetime. The coefficient functions  $B_l^p(r)$ , however, vanish for  $M \rightarrow 0$  and have the form

$$B_l^p(r) = a_l^p r^{-(p+2)} [1 + O(M/r)] , \quad (5)$$

where the coefficients  $a_l^p$  are proportional to  $M$ . (See [4] for additional details.)

The most interesting characteristic data on  $u = u_0$  correspond to two different cases: a) an initially static perturbation field for  $u \leq u_0$ , and b) a vanishing perturbation field for  $u \leq u_0$ . The first case corresponds to the collapse of an initially static star with an initially static perturbations. The second case corresponds to the collapse of an initially static star in which the collapse itself generates the perturbations.

One may also consider a more general (nonstatic) initial perturbation on  $u = u_0$ , but its generic effects can be modeled by the data on  $v = v_0$ , after reflection through the center. We shall see, on the other hand, that there is a qualitative difference in the tails if there is a static perturbation present initially.

We break the problem of evolution of the fields into two steps. In the first step we find  $\phi$  on  $u = u_1$ . This step requires the data on  $u = u_0$ , but only the early (small  $u$ ) data on the left boundary. In this step, then, the type of the left boundary (whether stellar center, surface of completely collapsing star, etc.) is unimportant. From the data on  $u = u_1$  we find  $\phi$  at late times, and at  $scri_+$ , in a second step. *To leading order in  $M$* , the evolution depends on the spacetime curvature in the first step, but not in the second step. The validity of this approximation is ultimately justified by numerical experiment.

We begin with the first step, the scattering in the region  $u_0 < u < u_1$ . We have taken the variation in  $\phi$  on  $v = v_0$  to be negligible after  $u_1$ . This means that, aside from backscattering, there is no outgoing radiation for  $u > u_1$ . In (4) the first series represents the non-backscattered waves, so our assumptions about no late outgoing waves are equivalent to taking  $G(u_1) = 0$ . For large  $r$  at  $u = u_1$  the dominant term in (4) is then

$$\Psi(u = u_1, r) = a_l^l r^{-l-2} G^{(-1)}(u_1) [1 + O(M/r)] , \quad (6)$$

where  $G^{(-1)}(u_1) \equiv \int_{u_0}^{u_1} G(u) du$ . The characteristic data, then, is proportional to the integrated initial burst, as well as to  $M$ . In the case of an initial static field, with the form

$$\Psi_{\text{static}} = \mu r^{-l} [1 + O(M/r)] , \quad (7)$$

the prediction is more definitive. In this case, at  $u = u_1$ , we have

$$\Psi = M\mu [(2l + 1)/(l + 1)] r^{-(l+1)} [1 + O(M/r)] . \quad (8)$$

(See again [4] for details.)

With this specification of characteristic data on  $u = u_1$  we can go on to consider the subsequent evolution of fields. We will show that the late time behavior of the fields at constant  $r$ , and the late-time behavior at  $scri_+$ , are independent of the details of the background at small  $r$ . The evolution is now the same in the spacetime geometry exterior to a star, a black hole, or to, e. g., an imploding-exploding shell of scalar field.

We confine our attention to the region  $u > u_1, r_* \gg M$ . The leading order effect on the propagation of  $\Psi$  is now that of the ‘‘centrifugal term’’  $l(l + 1)/r^2$  in  $V_l$ . In this sense we now approximate spacetime as flat. The solution for  $\Psi$  is then that of (4) with  $M = 0$ ,

$$\Psi(u, v) = \sum_{p=0}^l A_l^p r_*^{-p} \left[ (g^{(l-p)}(u) + (-1)^p f^{(l-p)}(v) \right] . \quad (9)$$

(To the approximation we are using here, for  $r_* \gg M$ , we have also  $r = r_*$ .) By matching this form to the initial data on  $u = u_1$  we find that

$$f(v) = F_0/v^P \quad (10)$$

where

$$F_0 = (-1)^l 2MG^{(-1)}(u_1), \quad P = 2, \quad (11)$$

if there is no initial static field, and

$$F_0 = (-2)^l 2M\mu [l!/(2l)!], \quad P = 1, \quad (12)$$

if there is an initial static field, with the form of (7). (These expressions involve a sum over the  $A_l^p$ , which are given in [4].)

We next take  $t \gg r_*$  and we expand  $g^{(k)}(u) = g^{(k)}(t) - g^{(k+1)}(t)r_* + \dots$ , and similarly for  $f(v)$ . By reordering terms we arrive at

$$\Psi = \sum_{n=-l}^{\infty} K_l^n r_*^n [f^{(l+n)}(t) + (-1)^n g^{(l+n)}(t)]. \quad (13)$$

The coefficients  $K_l^n$  are constructed from the  $A_l^p$  and vanish for  $l - n$  even,  $-l \leq n \leq l$ . We define  $h \equiv f + (-1)^l g$ , and we note that for  $t \gg r_*$   $\Psi$  has the form

$$\begin{aligned} \Psi = & K_l^{-l} h(t) r_*^{-l} + K_l^{-l+2} h''(t) r_*^{-l+2} + \dots \\ & + K_l^l h^{(2l)}(t) r_*^l + K_l^{2l+1} [2f^{(2l+1)}(t) - h^{(2l+1)}(t)] r_*^{l+1} + \dots \end{aligned} \quad (14)$$

We know that at late times  $f(v)$  has the power-law form given in (10); we make the *ansatz* that  $g(u)$  also falls off as a power law, so that we may write  $h(t) = H_0/t^N$ , where  $H_0$  is a constant.

We note that as  $t \rightarrow \infty$  the term  $h(t)r_*^{-l}$  will dominate if  $N < P + 2l + 1$  and the term  $2f^{(2l+1)}(t)r_*^{l+1}$  will dominate if  $N > P + 2l + 1$ . In either case only one of the constants  $H_0$  or  $F_0$  has an influence on the solution, and in fact the constant is simply an overall scaling of the solution. If either  $N < P + 2l + 1$  or  $N > P + 2l + 1$ , therefore, the form of the solution (aside from overall scaling) is fixed for  $r_* \gg M$ , its continuation to smaller values of  $r_*$  is fixed, and we cannot satisfy boundary conditions for small  $r$  (e.g., regularity at  $r = 0$  for a stellar model or, as  $r_* \rightarrow -\infty$ , at the horizon of a black hole). In order to satisfy a small- $r$  boundary condition we must have  $N = P + 2l + 1$  and hence

$$f(t) \simeq F_0 t^{-P}, \quad g(t) \sim (-1)^{(l+1)} F_0 t^{-P}, \quad (15)$$

$$h(t) \equiv f(t) + (-1)^l g(t) \sim 1/t^{P+2l+1}. \quad (16)$$

For  $M \ll r_* \ll t$  the form of the fields is particularly simple. In that case we have

$$\Psi = K_l^{2l+l} 2f^{(2l+1)}(t)r_*^{l+1} = -2K_l^{2l+l} F_0(P+2l)!t^{-(P+2l+1)}r_*^{l+1}, \quad (17)$$

and  $\Psi$  therefore falls off as  $1/t^{2l+2}$  (initial static field) or  $1/t^{2l+3}$  (no initial static field) at timelike infinity  $i_+$ . It follows from (15) and (9) that at  $scri_+$  (i. e., at  $v \rightarrow \infty$ ) we have

$$\Psi(v \rightarrow \infty, u) \simeq A_l^0 g^{(l)}(u) \simeq -A_l^0 F_0(l+P-1)!u^{-P-1}. \quad (18)$$

At null infinity  $scri_+$  the fields therefore fall off as  $u^{-l-1}$  (static initial field) or as  $u^{-l-2}$  (no static initial field).

We keep in mind that the above analysis did not depend on the small- $r$  details of the problem, and we go on to consider the specific case of a black hole. (It does not matter if it is eternal or formed in collapse, only that there is an internal “infinity”, i. e. an event horizon.) As  $r_* \rightarrow -\infty$  the curvature potential  $V_l$  in (3) is negligibly small and the solution to (3) can be written as  $\Psi = \alpha(u) + \gamma(v)$ . The nature of the characteristic data at  $v = v_0$  requires that  $\alpha(u)$  be a constant (aside from exponentially small variation) and with no loss of generality we choose it to be zero. For  $|r_*| \ll t$  we can then expand the solution, for large  $u$  and  $r_* \ll -M$  as

$$\Psi = \gamma(v) = \gamma(t) + \gamma'(t)r_* + \frac{1}{2}\gamma''(t)r_*^2 + \dots. \quad (19)$$

To join this solution, at  $r_* \ll -M$  to our previous solution in (17) for  $r_* \gg M$ , we make one further assumption. We assume that when  $t \gg |r_*|$  then, for the whole range of  $r_*$  (from  $r_* \ll -M$  to  $r_* \gg M$ ), the solution has the form  $\Psi \approx \Psi_{\text{finstat}}(r)/t^{P+2l+1}$ , where  $\Psi_{\text{finstat}}(r)$  is a  $t$ -independent solution of (3). This is clearly the case in the region  $t \gg r_* \gg M$ . With this assumption we can match the solution in (19) at  $r_* \ll -M$  and that in (17) for  $r_* \gg M$ , and conclude that  $\gamma(t) = \Gamma_0 t^{-P-2l-1}$ , and therefore that the late time behavior at the horizon is

$$\Psi(u \rightarrow \infty, v) = \gamma(v) = \Gamma_0 v^{-P-2l-1}. \quad (20)$$

The constant  $\Gamma_0$  is determined by the condition that there is a static solution  $\Psi_{\text{finstat}}$  such that



$$\lim_{r_* \rightarrow -\infty} \Psi_{\text{fnstat}}(r) = \Gamma_0, \quad (21)$$

$$\lim_{r_* \rightarrow \infty} \Psi_{\text{fnstat}}(r) = -2K_l^{2l+1} F_0(P+2l)! r^{l+1}. \quad (22)$$

The coefficient  $\Gamma_0$ , and therefore the behavior at the horizon, like all other aspects of the late time behavior, is fixed by the initial backscattering.

In the above analysis, we have seen that the backscattering of the initially outgoing waves, and the subsequent evolution in time, produces the power-law tails at  $scri_+$  and at future null infinity  $i_+$ . The small- $r$  nature of the background does not enter (except, of course, in the discussion of the tails at the horizon). This means that the same power-law tails should develop at  $scri_+$  and at  $i_+$  in models other than black hole models. We might consider as backgrounds: incompletely collapsing stars, static stars, imploding and exploding shells, and so forth. These different models would have different small- $r$  boundary conditions. All that is important to tail formation is that the source of the perturbations is sharply cut off as happens, due to the infinite redshift, in the black hole collapse case. We might consider, as an example, a quadrupole deformation of a nonrotating neutron star. A dynamical process might change the quadrupole perturbation from one static value to another (nonzero) static value. In this case, clearly, there cannot be a power-law fall off of the perturbation in time; the perturbation does not fall off at late times. On the other hand there might be a phase change in which the stellar crust loses the ability to support shear stresses responsible for the quadrupole moment, and the star might quickly become spherical. In this case, our analysis predicts that at late times the exterior quadrupole perturbation will fall off as  $1/t^6$ .

The only specific detail of our analysis that must be modified for non-hole models is the nature of the small- $r$  solution. In particular, the horizon condition in (19), (20), and (21) must be replaced by the appropriate small- $r$  condition, and the static solution  $\Psi_{\text{fnstat}}(r)$  is no longer the solution well behaved at  $r \rightarrow 2M$ , but rather the solution satisfying the appropriate small- $r$  condition (e.g., regularity at  $r = 0$ ). The result in (22) remains unchanged.

The analysis of perturbations on a Reissner-Nordström (RN) background, of mass  $M$  and charge  $Q$ , is very similar to that given above for the Schwarzschild background. For

scalar perturbations or for all radiative degrees of freedom of the mixed electromagnetic-gravitational perturbations, the field equations can be put in the form of (3), but with a potential of the form

$$V_l(r) = \frac{(r - r_+)(r - r_-)}{r^2} \left[ \frac{l(l+1)}{r^2} + R(r) \right], \quad (23)$$

where  $r_+, r_-$  are the radii of the outer and inner horizons

$$r_{\pm} = 2M \left( 1 \pm \sqrt{1 - (Q/M)^2} \right), \quad (24)$$

and where  $R(r)$  falls off as  $r^{-3}$ . The tortoise coordinate  $r_*$  for the RN background is the solution of

$$\frac{dr_*}{dr} = \frac{r^2}{(r - r_+)(r - r_-)} \quad (25)$$

for  $r_+ < r < \infty$ .

A review of the analysis of late time behavior for the Schwarzschild background confirms that almost all of the arguments depend on the general form of  $V_l(r)$  at large  $r$  and the exponentially sharp fall off of  $V_l(r)$  at the horizon. In these features there seems to be no difference between the Schwarzschild and the RN problems. The difference in the relationship of  $r$  and  $r_*$  in the two cases must be carefully considered, however; it is this relationship [not the details of  $R(r)$ ] that determines the initial backscattering and therefore the behavior of the late time tails. It turns out that there is no difference (for the tails) between the Schwarzschild and the RN cases. When the expression in (4) is substituted in (3) (with the RN form of  $u, v$  and  $V_l$ ) the result in (5) again emerges, and it is this result that determines the initial backscattering. The differences between the RN and Schwarzschild cases enter into the determination of  $B_l^p(r)$  only to higher order in  $r^{-1}$ .

### III. NUMERICAL METHOD

It is straightforward to integrate equation (3) on a  $uv$  null grid. The two-dimensional wave equation  $-4\Psi_{,uv} = V_l(r)\Psi$  is most simply discretized as

$$\Psi_N = \Psi_E + \Psi_W - \Psi_S - \Delta u \Delta v V_l \left( \frac{v_N + v_W - u_N - u_E}{4} \right) \frac{\Psi_W + \Psi_E}{8} + O(h^4). \quad (26)$$

Here the points N, S, E and W form a null rectangle with relative positions indicated by the points of the compass, and  $h$  is an overall grid scale factor, so that

$$\Delta u = u_N - u_E = u_W - u_S = O(h), \quad \Delta v = v_N - v_W = v_E - v_S = O(h). \quad (27)$$

Starting from null data on  $u = u_0$  and  $v = v_0$ , integration proceeds to the northeast (increasing  $v$ ) on one  $u = \text{const.}$  line after another.

The error estimate for  $\Psi_N$  follows directly if one assumes that the exact solution  $\Psi(u, v)$  has a Taylor expansion in the given null rectangle. On a grid of fixed total size in  $u$  and  $v$  there are  $O(h^{-2})$  grid points, so that the total error on the far end of the grid from the null data should scale as  $h^2$  when the grid size is scaled by  $h$ . We have done numerical tests which have confirmed this  $O(h^2)$  convergence.

The only difficulty in developing a code for this problem was the calculation of  $r$  from  $r_* = (v - u)/2$ . We have done it by iteration of the defining equation, in the form  $r = r_* - \ln(r - 1)$  for large  $r$ , and in the form  $r_1 = \exp(r_* - 1 - r_1)$  for  $r$  close to 1, that is, close to the horizon, where  $r_1 \equiv r - 1$ . We have used a grid of constant  $\Delta u = \Delta v$ . Because of the scale-invariance of the problem we have set  $2M = 1$ .

There is a small difference between the null data on  $u = u_0$  and  $v = v_0$  which we posed in the previous, analytical, section and our numerical work. For the numerical work, we posed *constant* data on  $v = v_0$ , and either generic (here Gaussian) or static data on  $u = u_0$ . The justification for this is the following. As we consider a linear wave equation, we can examine the evolution of data on  $v = v_0$  and of data on  $u = u_0$  separately. If we want to consider generic data on  $v = v_0$ , i. e. data which are localized, we can reflect them back at the scattering potential to get generic (although different data) on some  $u = \tilde{u}_0$ . So if we are not very interested in the exact shape of our data, putting them on  $u = u_0$  is sufficient.

#### IV. NUMERICAL RESULTS

We now report on the results of our numerical simulations of test fields on a Schwarzschild or RN background. Without loss of generality we have set  $2M = 1$ . As we are dealing with a linear wave equation, the overall amplitude of our initial data can also be chosen arbitrarily and is physically irrelevant. As our initial data null surfaces we chose  $v = 0$  for  $u \geq 0$  and  $u = 0$  for  $v \geq 0$ , which meet at the point  $t = 0$ ,  $r_* = 0$ . (The background is of course  $t$ -independent.)

In a first series of numerical experiments, we chose  $V_l(r)$  appropriate for a massless minimally coupled scalar field on a Schwarzschild background for different multipole indices  $l$ . It is of the form (3), with  $R(r) = 2M/r^3$ . As null data we used a Gaussian of width 3 centered at  $v = 10$  on  $u = 0$ .  $\Psi$  is chosen to be constant on the null boundary  $v = 0$ , with the constant determined by  $\Psi(u = 0, v = 0)$ . This is a simple approximation of the idea that the field is anchored in a star whose surface is rapidly redshifting, as explained in section II. We extended the grid from  $v = 0$  and  $u = 0$  to  $u = 400$  and  $v = 400$ , with a typical value of  $\Delta u = \Delta v = 0.1$ .

We examined the value of  $\Psi$  as a function of  $t$  on three lines, namely  $r_* = 10$ ,  $u = 400$  and  $v = 400$ . We took these lines as finite approximations of the future timelike infinity  $i_+$ , of the future horizon  $\mathcal{H}_+$  and future null infinity  $scri_+$ . Log-log plots of these three “tails” for  $l = 0$  are shown in Fig. 2. The predicted power-law behaviors are apparent for the case of an initial static field. On  $\mathcal{H}_+$  and  $i_+$  the field falls off as  $t^{-3}$ ; on  $scri_+$  the fall-off is as  $t^{-2}$ . The bend at the end of the  $scri_+$  line is not surprising. It represents null infinity only for  $v \gg u$ , which is no longer the case at that end of the line. The large wiggles at the left are a remnant of quasinormal ringing.

Quasinormal ringing is shown more clearly in the linear plot, for  $l = 1$  scalar perturbations, shown in Fig. 3. The agreement with the theoretically calculated frequency [7] is good. From the plot we read off values of 0.56 and  $-0.19$  for the real and imaginary parts of the frequency, for a scalar field with  $l = 1$ , for  $2M = 1$ . The predicted values [7] are 0.58587

and  $-0.19532$  for the least damped modes.

In Fig. 4 we show the effect of the multipole index  $l$  on the power law of the tail at  $i_+$ , again for a scalar field and Gaussian null data. The agreement of the power laws with the prediction is striking.

In a second series of numerical experiments we looked at the potential  $V_l$  appropriate for an electromagnetic field on a Schwarzschild background, which is (3) with  $R(r) = 0$ . We took null data corresponding to the initial presence of a static  $l$ -pole moment. (These are given in power-series form in [6], and we numerically evaluated the first few lowest orders in  $1/r$ .) The tails at constant  $r$  for  $l = 1$  and  $l = 2$  are shown in figure 5. (There is no electromagnetic monopole field.) It was shown in [4] how electromagnetic and spin-2 fields can be encoded in a scalar field. The potential  $V_l$  depends on the spin as well as on  $l$ , but the terms by which it differs for different spins are essentially Riemann tensor components and therefore of order  $2M/r^3$ . Terms of this order have been neglected in our analytic derivation, and the surprising prediction is therefore that the power law of the tails is independent of the spin of the testfield.

In a third series of experiments we examined a scalar test field on Reissner-Nordström backgrounds. The potential for a scalar field is now of the form (23), with  $R(r) = 2Mr^{-3} - 2Q^2r^{-4}$ . As explained in section III one expects the tails to be independent of the charge of the black hole. Figure 6 shows that this is in fact so, with the example of the tails at the (outer) horizon of an  $l = 0$  test field on Reissner-Nordström backgrounds with charge/mass ratios of  $Q^2/M^2 = 0.1$  and  $0.9$  respectively. This figure constitutes also direct evidence for the existence of power-law tails on the (outer) horizon for a generic perturbations, thus underpinning a central condition for the mass inflation scenario.

## V. CONCLUSIONS

When the dust of an approximately spherical collapse has settled, and spacetime inside the future lightcone of the collapse has approached Schwarzschild, Minkowski, or a stellar

interior spacetime, any massless fields that were present in the collapse still show “tails” that linger, decaying only as a power of time. In particular the  $l$ -th multipole moment of a massless test field decays like  $t^{-(2l+P+1)}$  at fixed radius at large times, with  $P = 1$  if there is an  $l$ -pole moment present before the collapse and  $P = 2$  otherwise. But power-law tails are also present on  $scri_+$ , where they decay like  $u^{-(l+P)}$ , and if a black hole has formed, on the horizon, where they decay like  $v^{-(2l+P+1)}$ . The amplitude of the tails can be calculated as a function of the initial multipole moment, and in its absence, as an integral over the radiation going out to infinity during the collapse.

Neither this amplitude, nor the exponent of the power law, depend upon the spin of the massless field in question, nor, if the black hole is charged, on its charge. We have shown the origin of these features in an analysis which is based on [4]. The spin- and charge-dependent parts of the effective radial potential of a massless test field on a Reissner-Nordström background are of an order that can be neglected in this analysis.

We have checked numerically that the tails are indeed present on null infinity and the horizon, and are independent of the spin of the field and the black hole charge. The fact that power-law tails are present on the outer horizon of a Reissner-Nordström black hole after a generic collapse situation is of crucial importance to the mass inflation scenario. It has, to our knowledge, never been demonstrated explicitly.

Finally, one decisive step of our analysis was a regularity condition, either on the horizon when a black hole formed in the collapse, or else at the center of spherical symmetry. This argument generalizes to any kind of boundary condition posed at small radius, and strongly suggests that perturbations of massless fields outside any spherical background object should also have power-law tails with the powers given above. In a subsequent paper we report results for a closely related *nonlinear* problem: the implosion of a shell of scalar field.

We wish to thank Josh Goldberg and Fritz Rohrlich for pointing out early references. This work was supported in part by grant NSF PHY92-07225 and by research funds of the University of Utah. J.P. acknowledges hospitality and support from the Institute for Theoretical Physics at UCSB and the National Science Foundation grant PHY89-04035.

## REFERENCES

- [1] B. S. DeWitt and R. W. Brehme, *Ann. Phys. (NY)* **9**, 220 (1960).
- [2] F. Rohrlich and J. Winicour, in *Perspectives in Geometry and Relativity, Essays in Honor of Václav Hlavatý* (University of Indiana Press, 1966) (see correction in ref. [3]).
- [3] F. Rohrlich, *Classical charged particles* (Addison Wesley, Reading, 1990).
- [4] R. H. Price, *Phys. Rev. D* **5**, 2419 (1972).
- [5] T. M. Helliwell and D. A. Konkowski, *Phys. Rev. D* **47**, 4322 (1993) and references therein.
- [6] C. T. Cunningham, V. Moncrief, and R. H. Price, *Astrophys. J.* **224**, 643 (1978).
- [7] E. Leaver, Ph. D. Thesis, University of Utah (1985) (unpublished).
- [8] T. Apostolatos, D. Kennefick, A. Ori, and E. Poisson, *Phys. Rev. D* **47**, 5376 (1993).
- [9] K. Thorne, in *Magic without Magic*, J. R. Klauder, ed. (W. H. Freeman, San Francisco, 1972)

## FIGURES

Fig. 1: Spacetime of a collapsing spherically symmetric star. Outside the star the metric is Schwarzschild. Coordinates  $t$ ,  $r_*$ ,  $u$  and  $v$  are indicated.

Fig. 2: Log-log plots of a spherically symmetric scalar test field on Schwarzschild spacetime. The initial data were Gaussian.  $\phi(r = 10, t)$  represents future timelike infinity.  $\phi(u = 400, v)$  represents the future horizon.  $\phi(v = 400, u)$  represents future null infinity. The power-law exponents are  $-3.08$  on  $i_+$  and  $-3.02$  the horizon, and  $-2.11$  on  $scri_+$ .

Fig. 3:  $\phi(r = 10, t)$  plotted for a scalar testfield with angular dependence  $l = 2$  on Schwarzschild spacetime, showing quasinormal ringing. The initial data are Gaussian.

Fig. 4: Log-log plots of  $\phi(r = 10, t)$  for scalar testfields with angular dependence  $l = 0, 1, 2$ , showing power-law exponents  $-3.03$ ,  $-4.99$ , and  $-6.94$ . Gaussian initial data.

Fig. 5: Electromagnetic test field, with angular dependence  $l = 1, 2, 3$  on Schwarzschild background. Plotted is the field at  $u = 400$  versus  $v$ , representing the horizon. Static-static initial data. The power-law exponents are  $-4.95$  and  $-5.93$  and  $-8.63$ .

Fig. 6: Scalar test field on RN background, shown on "horizon". Gaussian initial data with  $l = 0$ . Shown are charge/mass ratios  $Q^2/M^2 = 0.1$  and  $0.9$ . The power laws are  $-3.18$  and  $-3.17$ .



Figure 1

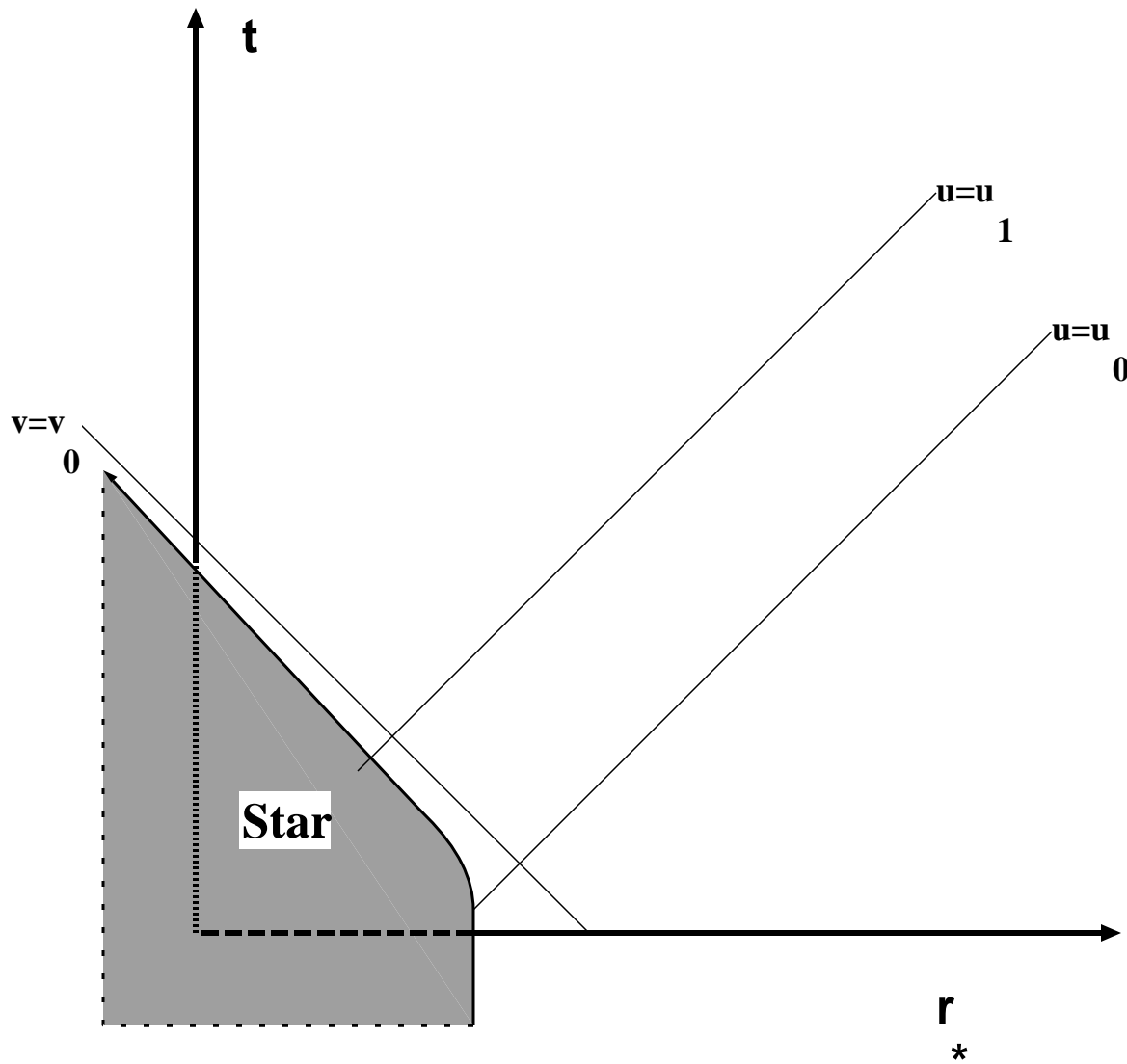


Fig. 2

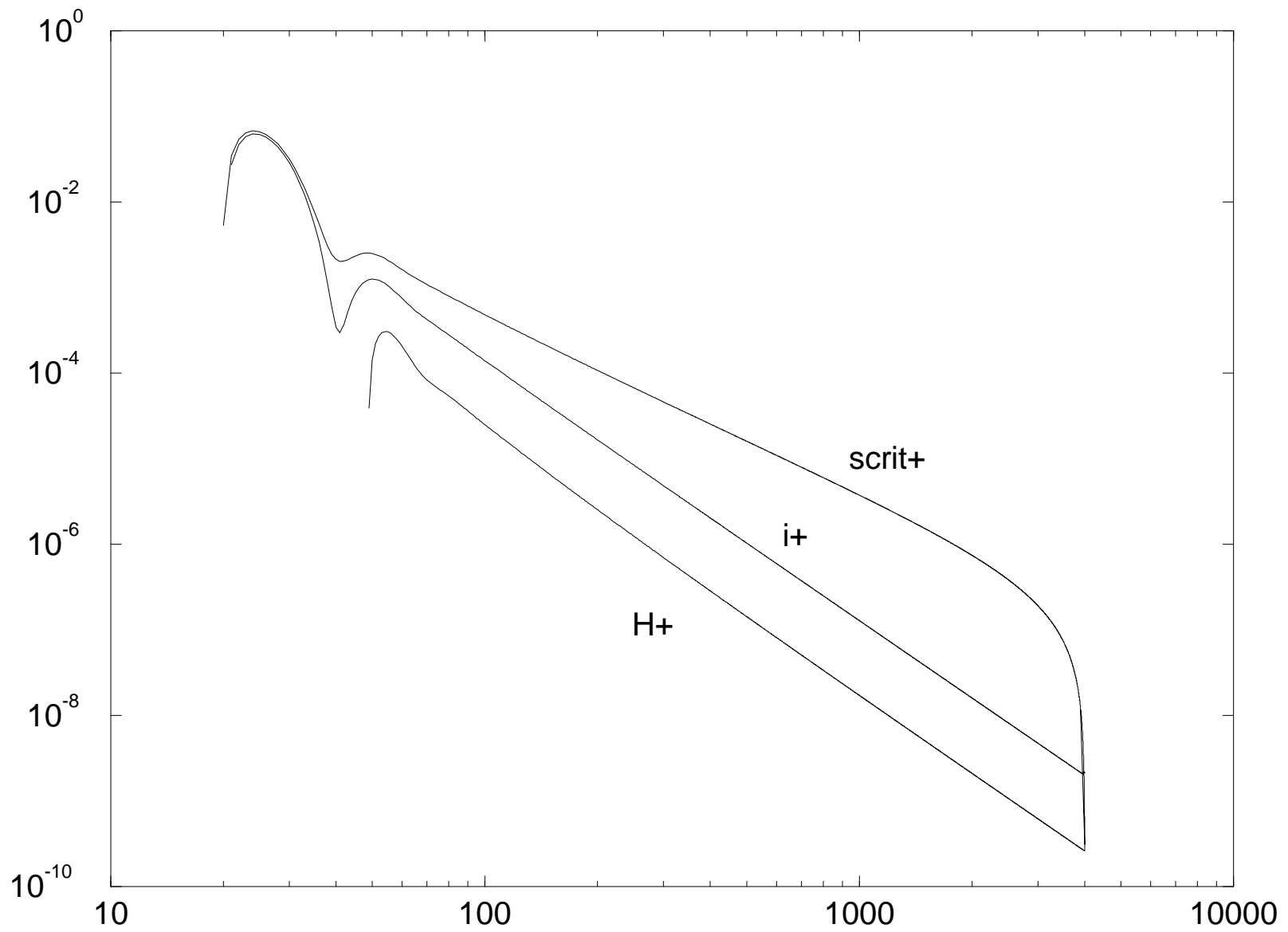


Fig. 3

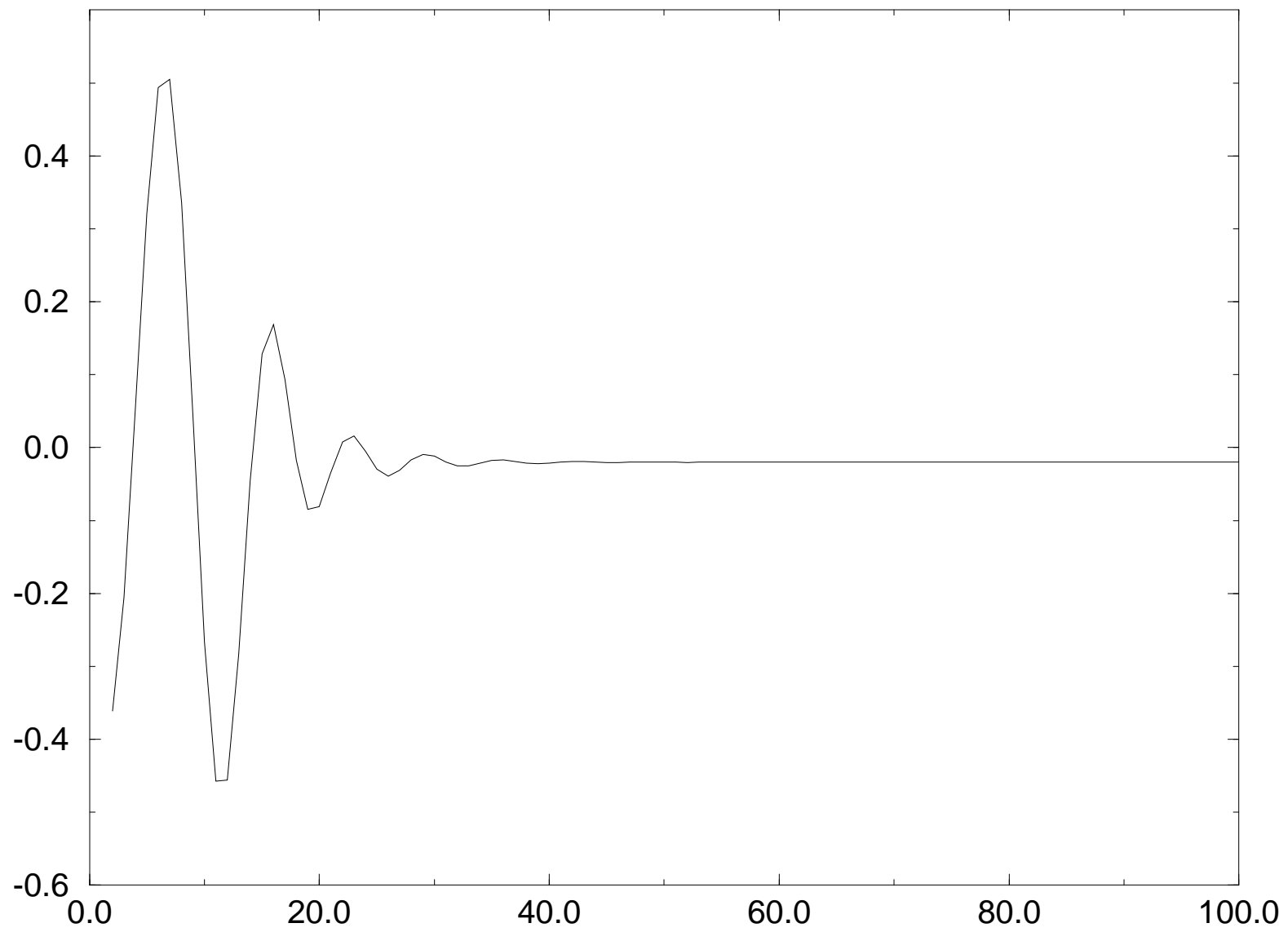


Fig. 4

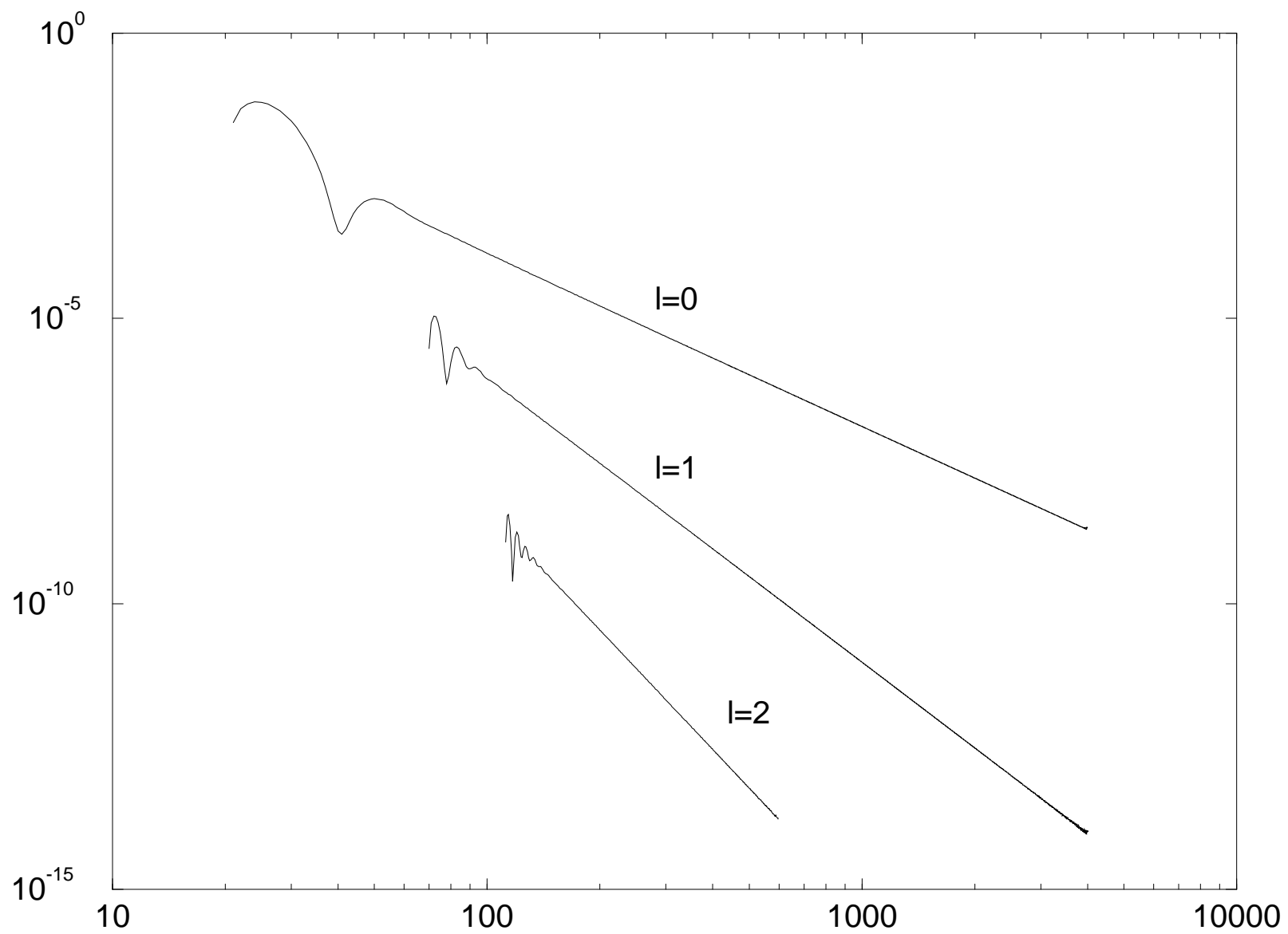


Fig. 5

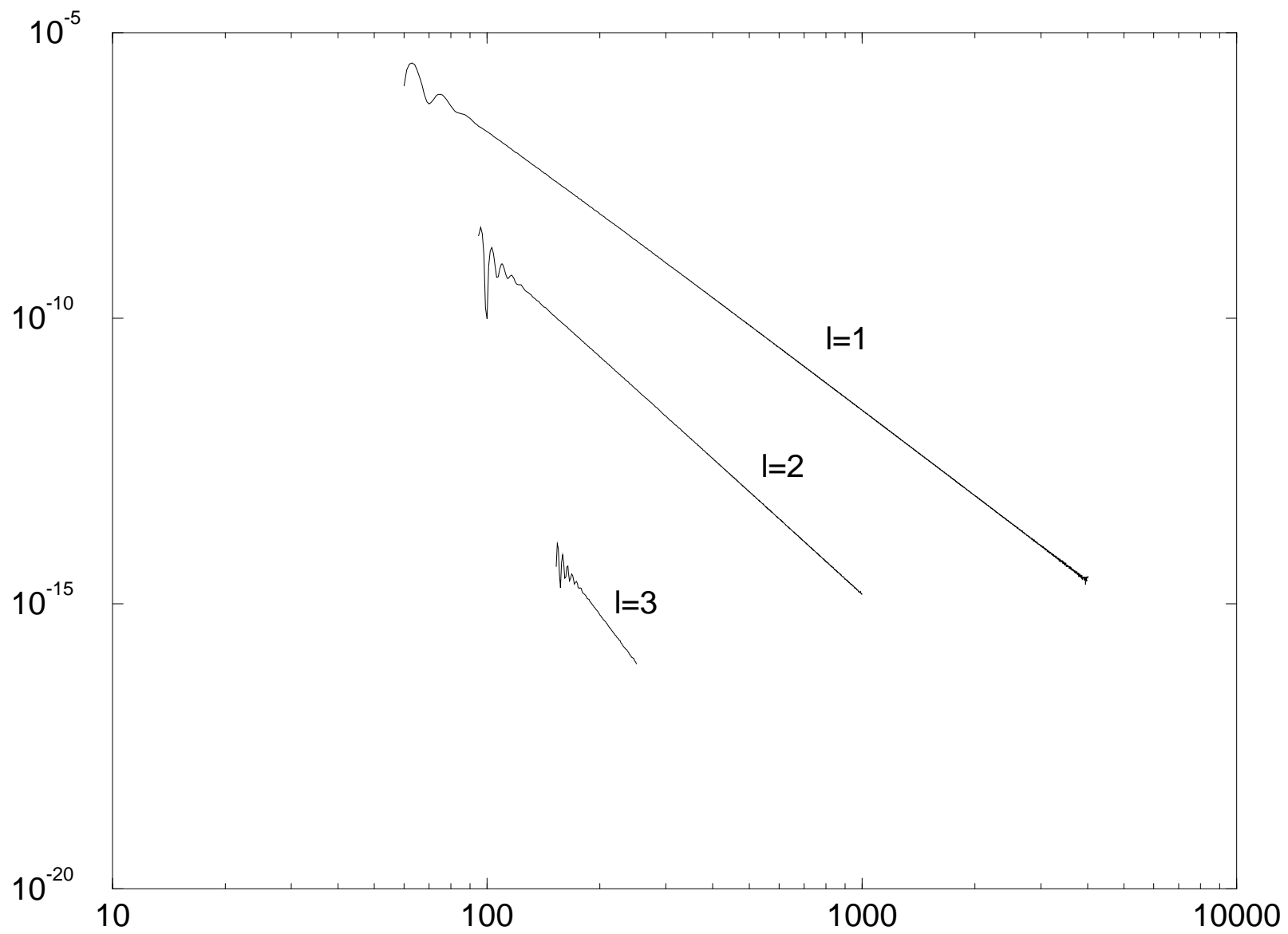


Fig. 6

